Key Role of Active-Site Water Molecules in Bacteriorhodopsin Proton-Transfer Reactions

Ana-Nicoleta Bondar,*,†,‡,§,∥ Jerome Baudry,⊥,# Sándor Suhai,‡ Stefan Fischer,▽ and Jeremy C. Smith*,⊥,#

Computational Molecular Biophysics, IWR, University of Heidelberg, Im Neuenheimer Feld 368, D-69120 Heidelberg, Germany, Molecular Biophysics Department, German Cancer Research Center, Im Neuenheimer Feld 580, D-69120 Heidelberg, Germany, University of California at Irvine, Department of Physiology and Biophysics and the Center for Biomembrane Systems, Med. Sci. I, D-374, Irvine, California 92697-4560, University of Tennessee/Oak Ridge National Laboratory Center for Molecular Biophysics, Oak Ridge National Laboratory, PO BOX 2008 MS6164, Oak Ridge, Tennessee 37831-6164, Department of Biochemistry and Molecular Biology, University of Tennessee, M407 Walters Life Sciences, 1414 Cumberland Ave, Knoxville Tennessee 37996, and Computational Biochemistry, IWR, University of Heidelberg, Im Neuenheimer Feld 368, D-69120 Heidelberg, Germany

Received: March 4, 2008; Revised Manuscript Received: August 20, 2008

The functional mechanism of the light-driven proton pump protein bacteriorhodopsin depends on the location of water molecules in the active site at various stages of the photocycle and on their roles in the proton-transfer steps. Here, free energy computations indicate that electrostatic interactions favor the presence of a cytoplasmic-side water molecule hydrogen bonding to the retinal Schiff base in the state preceding proton transfer from the retinal Schiff base to Asp85. However, the nonequilibrium nature of the pumping process means that the probability of occupancy of a water molecule in a given site depends both on the free energies of insertion of the water molecule in this and other sites during the preceding photocycle steps and on the kinetic accessibility of these sites on the time scale of the reaction steps. The presence of the cytoplasmic-side water molecule has a dramatic effect on the mechanism of proton transfer: the proton is channeled on the Thr89 side of the retinal, whereas the transfer on the Asp212 side is hindered. Reaction-path simulations and molecular dynamics simulations indicate that the presence of the cytoplasmic-side water molecule permits a low-energy bacteriorhodopsin conformer in which the water molecule bridges the twisted retinal Schiff base and the proton acceptor Asp85. From this low-energy conformer, proton transfer occurs via a concerted mechanism in which the water molecule participates as an intermediate proton carrier.

Introduction

Water molecules are believed to be key components of proton-pumping proteins.[1−9] Water molecules can influence the geometry and the proton affinity of the protein amino acid groups to which they hydrogen bond, or act as intermediate proton carriers. It is thus essential, when investigating proton-pumping mechanisms, to determine the roles of specific water molecules and how they change location as the protein passes through the intermediate states of the pumping cycle.

An example of a proton-pumping protein whose functioning is intimately connected to water molecules is bacteriorhodopsin, a light-driven proton pump from the *Halobacterium salinarium* purple membrane.[10] In the resting state "bR" of the pump, water molecule w402 hydrogen bonds to the protonated retinal Schiff base, to Asp85, and to Asp212, in doing so stabilizing the protonated state of the Schiff base[11,12] (Scheme 1). Active-site water molecules are central to various scenarios proposed for the first proton-transfer step, which is from the retinal Schiff base to Asp85.[13−17] Water molecules hydrogen bonding to the proton donor or acceptor groups have a significant effect on the energetics of retinal proton-transfer reactions.[18−20] In the cytoplasmic channel, water molecules mediate the long-distance proton transfer from Asp96 to the Schiff base;[21−23] in the extracellular channel, water molecules are critical for storing and releasing a proton to the extracellular side of the membrane.[8,24]

The first proton-transfer step of bacteriohodopsin, in which a proton is transferred from the retinal Schiff base to Asp85,

SCHEME 1: Location of Water Molecule w402 and the Cytoplasmic Water B Relative to the Retinal Schiff Base[a]

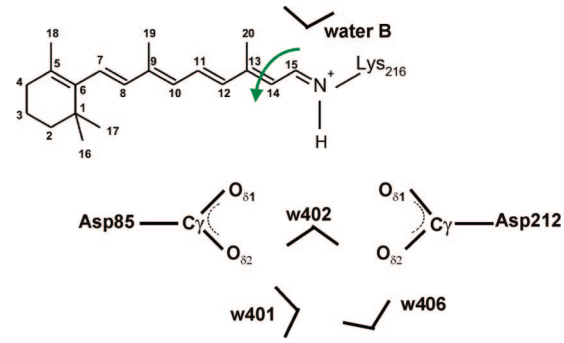

[a] For simplicity, retinal is depicted here in the all-trans configuration, and the isomerizing C_{13}=C_{14} bond is indicated by the green arrow.

* Corresponding authors. E-mail: nicoleta.bondar@uci.edu (A.-N.B.); smithjc@ornl.gov (J.C.S.).
† Computational Molecular Biophysics, IWR, University of Heidelberg.
‡ German Cancer Research Center.
§ University of California at Irvine.
∥ Present address: University of California at Irvine, Department of Physiology and Biophysics, School of Medicine, Med. Sci. I, D374, Irvine, CA 92697-4560.
⊥ Oak Ridge National Laboratory.
University of Tennessee.
▽ Computational Biochemistry, IWR, University of Heidelberg.

10.1021/jp801916f CCC: $40.75
Published on Web 10/31/2008

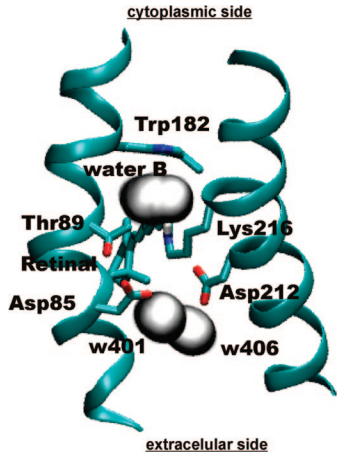

Figure 1. Dynamics of water molecule B. The gray ellipsoids indicate the locations sampled by the oxygen atoms of water B, w401, and w406, during the 500 ns production run of the classical Langevin MD simulation at 150 K started from the crystal structure of ref 5. The picture was prepared using the VMD software.[95]

has been extensively investigated by experimental and theoretical approaches (see, e.g., refs 15−19 and 25−28). Nevertheless, the exact role of the water molecules in retinal deprotonation remains an outstanding open question. The need to understand the location and role of water in retinal deprotonation was reinforced by recent solid-state NMR experiments[15] indicating a strong interaction between the twisted L-state retinal Schiff base and its counterion, which could be a highly polarized water molecule. This observation led to the question of whether bacteriorhodopsin may act as an inward hydroxyl pump, rather than an outward proton pump.[27]

The molecular picture of the geometry of the twisted retinal Schiff base strongly interacting with its counterion in L is not clear. Three crystal structure models of the L intermediate indicate a water molecule in the close vicinity of the retinal Schiff base.[13,14,28] In two of these structures, the retinal Schiff base has an extracellular orientation, with the Schiff base C_{15}═N bond either syn[28] or trans.[13] In the third structure, retinal is 15-anti with the Schiff base in a cytoplasmic orientation.[14] The 15-syn retinal conformer of ref 28 is unlikely to participate in proton transfer because other spectroscopic results indicate that retinal is 15-anti along the reaction cycle,[29] and the energy barriers for the formation of 15-syn from K, and for the reprotonation of the Schiff base from Asp96, are significantly higher than expected from the known kinetics of the reaction cycle.[30,31] The 15-anti conformer with extracellular-oriented Schiff base[13] (PDB[32] code 2NTW) indicates an angle for the C_{13}═C_{14} dihedral of −107.9°; it has been noted that the retinal twist and the interaction between the Schiff base and water in this structure are difficult to reconcile with NMR[15] and FTIR data, respectively.[17]

The L-state model in which the 15-anti retinal has a cytoplasmic-oriented Schiff base hydrogen bonded to a water molecule[14] (see water B in Figure 1) appears to agree best with FTIR[17,33] and dipole-moment measurements.[34] The cytoplasmic orientation of the retinal Schiff base prior to proton transfer is supported by two other crystal structures of a putative L state,[35,36] FTIR observations,[17] and computations.[16,37] However, it is not clear to what extent the interactions between the Schiff base and the water in the crystal structure of ref 14 are sufficient to explain the observations from NMR that in L there is a strong interaction between the Schiff base and its counterion.[15]

The proposal of a cluster of water molecules on the cytoplasmic side of the L-state retinal Schiff base[17,33] has also been debated. A comparison between the FTIR spectral fingerprints of water at 170 K vs room temperature led to the conclusion that the water-filled cavity on the cytoplasmic side of the retinal Schiff base may be present only at low temperatures, and the alterations in the low-temperature L may be due to a dynamical transition in the bacteriorhodopsin purple membrane at ∼170 K.[26] It had been argued in ref 17 that the discrepancies between the data on the water molecules on the cytoplasmic side of the L-state retinal in refs 17 and 26 are caused by differences in the experimental protocols, which presumably would have perturbed the photocycle in ref 26. A recent study in which the dynamical transition in bacteriorhodopsin purple membrane was studied by neutron scattering experiments and molecular dynamics (MD) simulations indicated inflections in the mean-squared displacements of the purple membrane at 120 and 260 K, and at 200 and 260 K for the hydration water.[38]

X-ray crystallography provides invaluable information on the protein, retinal, and water geometries that may be sampled during the reaction cycle. However, crystallographic information on the hydration of protein internal cavities obtained from data at limited resolution needs to be considered with caution, as it may be subject to artifactual electron density arising from the atoms surrounding the cavity.[39] Mobile and/or low-occupancy water molecules are difficult to characterize with X-ray crystallography.[40] In the case of nonpolar protein internal cavities, the crystallographic information on hydration may be affected by the equilibrium water occupancy being lower at the cryogenic temperatures used to solve the crystal structures than at room temperature.[41] Indeed, recent molecular dynamics (MD) simulations have been interpreted to suggest that at room temperature the number of internal water molecules transiently present in bacteriorhodopsin is much greater than indicated by the crystal structures.[42]

Another essential aspect in discussing the retinal geometry and its interactions with water is that retinal and water are dynamic molecules, whereas the crystal structures provide single configurations. MD simulations demonstrated that retinal is flexible, and as such, it samples a relatively large range of dihedral angle values in the protein environment.[36,43−45] Proton-transfer computations indicated that the strong attractive interactions between the protonated Schiff base and the negatively charged Asp85, and flexibility of the retinal chain and of the surrounding protein groups, enable the proton donor and acceptor groups to come to within proton-transfer distance without a significant energetic penalty.[16,30] The critical role of the electrostatic interactions for bacteriorhodopsin's proton-transfer reactions has been demonstrated in careful theoretical work.[25,46] The flexibility of the retinal chain and the attractive interactions between the Schiff base and Asp85 could explain the transient sampling of conformers with the Schiff base hydrogen bonded to either Asp85 or Thr89 in classical MD simulations starting from an L-state model with planar, cytoplasmic-oriented 15-anti retinal.[36]

Here, we contribute to the understanding of the role of water in bacteriorhodopsin proton pumping by using computer simulations to address the following open questions: (i) is the presence of a water molecule (labeled here as water B) in the cavity on the cytoplasmic side of the retinal Schiff base allowed on thermodynamic grounds; (ii) can we derive a molecular picture of the active site in which a twisted 13-cis,15-anti retinal interacts strongly with the counterion, as proposed on the basis of solid-state NMR;[15] (iii) what is the proton-transfer mechanism for the geometry of the active site described in question ii. To

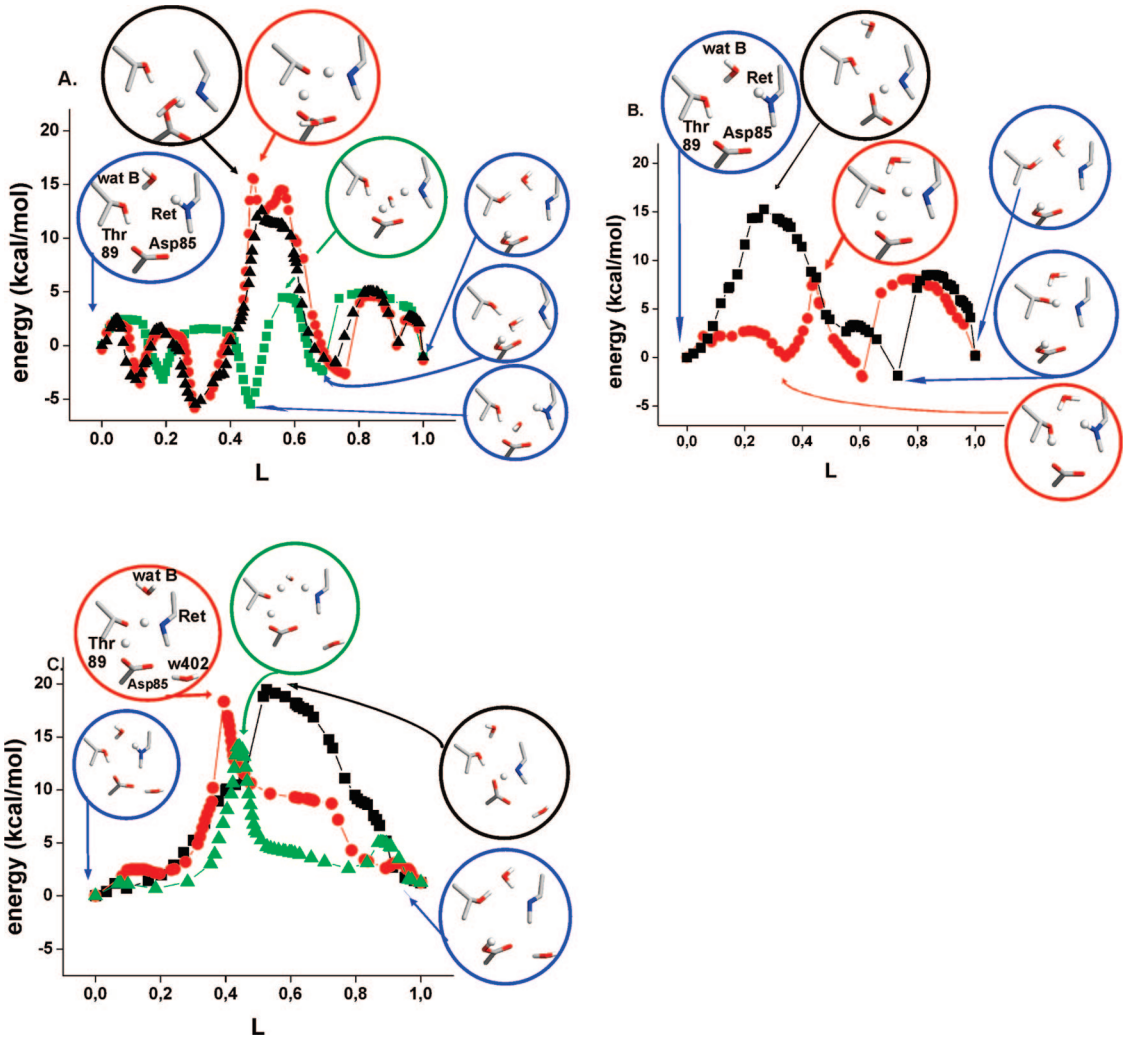

Figure 2. Influence of the cytoplasmic water molecule B on the proton-transfer mechanism in the absence (A,B) and in the presence (C) of water molecule w402. The energy profiles for proton transfer via water B (path **1a**) or Thr89/water B (path **2a**), Thr89 (path **1b**, **1b′**, and **2b**), and directly to Asp85 (paths **1c**, **1c′**, and **2c**) are depicted with green, red, and black, respectively. The paths in panels A and B differ in that paths in panel B do not involve the passage through the low-energy conformer at $L = 0.46$ in Figure 2A, green curve. Insets give the geometries in the reactant, product, the rate-limiting transition states, and the local minima discussed in the text. The insets are encircled in light blue for the end states and local minima common to the paths depicted in the same panel; insets are encircled in the color of the corresponding energy profile for the rate-limiting saddle points. The transferring protons are depicted as small spheres. The reaction coordinate L gives the sum along the entire path of the changes in all atomic coordinates calculated as a root-mean-squared difference.[69] At $L = 0$, the Schiff base is protonated and Asp85 is negatively charged, and at $L = 1$, Asp85 is protonated and the Schiff base is neutral. The energies are QM/MM-optimized values given in kcal/mol, taken relative to the conformation at $L = 0$.

address these questions, we employ classical molecular mechanics (MM) and combined quantum mechanical/molecular mechanical (QM/MM) MD simulations, free energy computations for water insertion, and potential of mean force and minimum-energy reaction-path calculations for proton transfer.

Methods

Structural Models Used. The molecular mechanical (MM) free energy computations were performed using the L-state model of ref 14 for the starting coordinates. The reaction-pathway calculations discussed in conjunction with the reaction network diagram were computed using the coordinates from refs 11, 13, 22, 28, 35, 47, and 48. Coordinates for the missing internal residues and the hydrogen atoms were constructed using the CHARMM software.[49] Protein amino acid residues 5−231 and all internal crystallographic water molecules were included in the calculations. The N- and C-termini were capped with the neutral groups CH_3-CO- and $-NH-CH_3$, respectively. Amino acid residues Asp96 and Asp115 were considered protonated.[50] The extracellular proton release group, which includes water molecules, Arg82, Glu194, and Glu204[8,51] was modeled by protonating Glu204. Standard protonation states were assumed for all remaining protonatable protein groups.

In all calculations, part of the protein atoms was mobile while the remaining atoms were fixed to their coordinates from the crystal structures. The mobile region consisted of approximately 830 atoms comprising retinal, one layer of protein groups and water molecules, and other protein groups and water molecules whose flexibility might be coupled to the events in the active site. The structural models were energy-optimized to a gradient of 10^{-3} kcal/mol/Å using the potential energy function described below. The energy optimizations were performed by placing harmonic constraints on the heavy atoms, and progressively weakening the constraints from 10 to 1 kcal/mol with a step size of 1 kcal/mol, and from 1 to 0 kcal/mol with a step size of 0.1 kcal/mol.

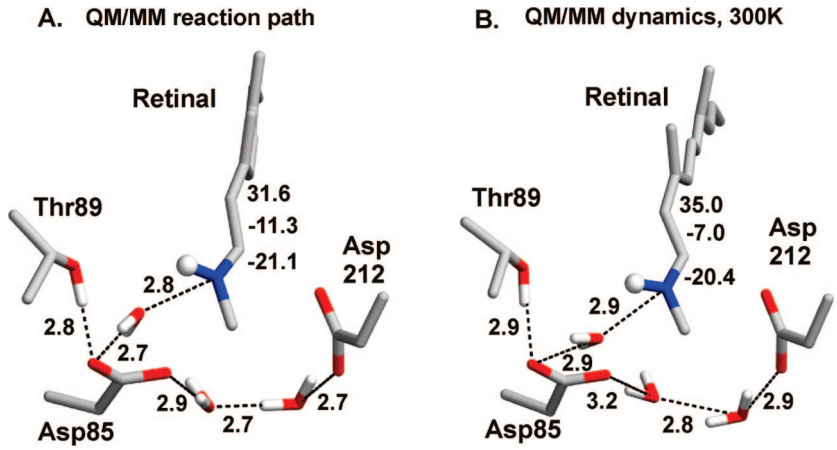

Figure 3. Schiff base, counterion, and water interactions. Schematic representation of the retinal Schiff base region in the low-energy conformer from QM/MM-optimized reaction-path calculation (panel A), and at the end of the QM/MM MD simulation at 300 K (panel B). The conformer in Figure 3A is taken from path **2a**, $L = 0.46$, green curve in Figure 2A. The broken lines indicate hydrogen bonds, with distances given in angstroms. The numbers by the retinal bonds C_{13}═C_{14}, C_{14}—C_{15}, and C_{15}═N give the deviation of the main-chain dihedral angles relative to the planar geometry, in degrees. See Scheme 1 for the numbering of the retinal atoms.

Potential Energy Function. The free energy perturbation calculations were performed by describing the retinal, protein, and water molecules with MM. We used the CHARMM27 parameter set for the protein,[52] the TIP3P model for water,[53] and the parameter set adjusted in ref 54 based on refs 44 and 55 for the retinal moiety.

All reaction-path calculations and an additional set of MD simulations were performed using the combined quantum mechanical/molecular mechanical (QM/MM) approach.[56−58] The QM/MM treatment for bacteriorhodopsin proton transfer was described in detail in ref 20. Briefly, the active-site groups (retinal, the Asp85, Thr89, Thr89, and Lys216 side chains, and w402) are described with quantum mechanics, with the hydrogen link atom[56] attached to the C_α atoms of the aspartate and threonine groups, and to the C_β atom of Lys216. When present, the cytoplasmic water molecule B was treated with QM. The remaining protein groups and water molecules were treated with MM using the parameters from refs 52, 53, and 59 The interactions between the QM electrons and nuclei were computed using the self-consistent-charge density-functional tight binding method (SCC-DFT60[60]). The bonded (bond, angle, dihedral, and improper angles) and nonbonded (Coulombic and van der Waals) interactions between the MM atoms and between the MM and QM atoms were computed with the CHARMM force field,[49] and the QM/MM implementation of SCC-DFTB.[61] The nonbonded interactions were smoothly brought to zero by multiplying by a cubic switch function from 7 to 14 Å. A relative dielectric constant of 1 was employed.

Comparisons of SCC-DFTB with higher-level QM methods indicated that SCC-DFTB is reliable in describing the geometry and energetics of test hydrogen-bonded systems, and gave good agreement with B3LYP in describing the geometry and relative energetic ordering of various conformations of model peptides.[62] Compared to B3LYP/6-31G*, SCC-DFTB gives a reasonable description of retinal's geometry and torsional properties.[63]

In conjunction with a QM/MM approach, SCC-DFTB has been used to investigate proton transfer in, e.g., triose phosphate isomerase,[61] carbonic anhidrase II,[64] yeast cytosine deaminase,[65] cytidine deaminase,[66] and bacteriorhodopsin.[16,30] Comparison with higher-level methods indicated that SCC-DFTB gives a reasonable description of structures and energetics of proton transfer in these systems. In the case of triose phosphate isomerase, the SCC-DFTB energetics agreed with B3LYP/6-31+G** to within 2−4 kcal/mol (rms values).[61] Good agreement between SCC-DFTB and higher-level B3LYP and MP2 calculations was found in benchmark calculations on protonated two- and three-membered water clusters, and active-site models of carbonic anhydrase in the gas phase.[64] For these active-site models, the SCC-DFTB reaction energy was between −5.6 and −7.5 kcal/mol, as compared to values between −3.8 and −5.7 with B3LYP/6-31+G**; the proton-transfer barrier had values between 2.1 and 3.9 kcal/mol with SCC-DFTB, and between 3.5 and 5.8 kcal/mol with B3LYP/6-31+G**.[64]

SCC-DFTB with a specific parametrization for the retinal Schiff base was found to agree to within 1 and 4 kcal/mol with B3LYP/6-31G** and MP2/6-311+G**, respectively, in describing the relative deprotonation energy of retinal and acetate models in the gas phase.[20] For the low-energy proton-transfer paths in bacteriorhodopsin, the rate-limiting barriers of the SCC-DFTB/MM-optimized paths were within 2.1 kcal/mol (rms values) from values recalculated with B3LYP 6-31G**/MM without reoptimizing the SCC-DFTB/MM paths;[16] the reaction energies computed with SCC-DFTB/MM and B3LYP 6-31G** agreed to within 2 kcal/mol. Moreover, a full B3LYP 6-31G**/MM optimization of a pair of reactant and product states of proton transfer indicated an energy difference (reaction energy) of 2.6 kcal/mol, in good agreement with the 0.8 kcal/mol value found by energy-optimizing with SCC-DFTB/MM the same pair of end states.[20] The agreement between the active-site geometries in this pair of conformers optimized with SCC-DFTB/MM and B3LYP 6-31G**/MM was excellent, the largest differences being the overestimation of the Schiff base:Thr89 hydrogen-bonding distance by 0.11 Å, and the underestimation of the C_{14}—C_{15} bond twist by 7°, in the structure of a protonated Schiff base/negatively charged Asp85 conformer optimized with QM/MM DFTB.[20]

Reaction-Path Calculations. The proton transfer from the retinal Schiff base to Asp85 during the transition between the intermediate states L and early-M steps occurs on a time scale of ∼10 μs, which cannot be addressed via direct QM/MM molecular dynamics simulations. Because the structural changes associated with retinal deprotonation are confined mainly to the Schiff base region,[13,14,16,28,36,47] there are no significant protein conformational changes in the first half of the bacteriorhodopsin reaction cycle,[67] and the energetics of the primary proton transfer step is dominated by enthalpy,[68] as a first approximation

minimum-energy reaction pathways can provide valuable information into the proton-transfer mechanism. The conjugate peak refinement algorithm (CPR[69]) was used successfully in the investigation of chemical reactions and conformational transitions in systems with many degrees of freedom.[16,54,70,71] The CPR algorithm does not require the a priori knowledge of the reaction path, which could be difficult in the case of bacteriorhodopsin.[20,72] Instead, CPR builds and optimizes the pathway by starting from energy-optimized models of the reactant- and product-state structures. The optimization of the pathway is complete when all energy maxima along the pathway are first-order saddle points, which give the transition states of the reaction. The reactant, product, and local minima were energy-optimized to a gradient of 10^{-3} kcal/mol/Å.

To further explore the potential energy surface and reduce the limitations inherent to any minimization-based approach (the path may depend somewhat on the initial conditions), different reactant, product, and putative intermediate states can be considered. The analysis of the transition states from the CPR path provides information about the rate-limiting energy barrier and the sequence of structural changes leading from the reactant to the rate-limiting transition state, and from the rate-limiting transition state to the product state.

Free Energy Perturbation Calculations. We used the methodology described in ref 23 to compute the free energy of inserting water molecule B. Previous calculations based on that methodology[23] led to the suggestion that the presence of a water molecule hydrogen bonding to the all-trans retinal Schiff base in the bR state is thermodynamically permitted;[23,55,74] ab initio computations indicated that strong hydrogen-bonding interactions with the retinal could stabilize water molecules in the retinal binding site on either site of the protonated retinal Schiff base.[73] This result is consistent with high-resolution X-ray crystallographic structures of the bR state, which indicated coordinates for the water molecule w402 hydrogen bonding to the retinal Schiff base (Scheme 1).[11,12]

In the first step of the free energy calculations, the system is equilibrated by performing classical molecular dynamics simulations. From the molecular dynamics simulations, the average (reference) location of the water molecule is extracted. A force constant k_{harm} of the harmonic potential acting on the water molecule is then computed according to the equation

$$k_{\mathrm{harm}} = \frac{3k_{\mathrm{B}}T}{\langle \delta r^2 \rangle} \tag{1}$$

where k_{B} is the Boltzmann constant, T is the absolute temperature, and $\langle \delta r^2 \rangle$ is the mean square fluctuation of the water oxygen atom.[23]

The force constant k_{harm} is employed to apply a harmonic restraint potential on the water molecule during the next two stages of the free energy calculation, which are as follows. First, the water molecule is gradually removed by progressively turning off the electrostatic and then the van der Waals interactions. Second, the water molecule is inserted back by gradually turning on the van der Waals energy term, and then the electrostatic interactions. The perturbation windowing thermodynamic integration method[75,76] was used to compute the free energy increments $\Delta A(\lambda, \lambda + \delta\lambda)$ at values of the coupling parameter $\lambda = 0.05, 0.15, ..., 0.95$, perturbed by ± 0.05.[23] At each value of λ, the system was first equilibrated and then a production run performed. Finally, the probability of occupancy of the water molecule inserted at a given location was computed as

$$P = \frac{R}{R+1} \tag{2}$$

where the binding factor R of the water molecule is

$$R = \rho_{\mathrm{bulk}} \left(\frac{2\pi k_{\mathrm{B}}T}{k_{\mathrm{harm}}} \right)^{3/2} \mathrm{e}^{-|\Delta A^{0\rightarrow 1}_{cavity} - \Delta A^{0\rightarrow 1}_{bulk}|/k_{\mathrm{B}}T} \tag{3}$$

with ρ_{bulk} the bulk water density, $\Delta A_{\mathrm{cavity}}$ the free energy for inserting the water molecule in the protein cavity, and ΔA_{bulk} the free energy for inserting a TIP3 water molecule in the original location of the water (e.g., bulk water[23]).

To investigate the thermodynamic permissibility of the cytoplasmic water molecule B, the L-state model of ref 14 was first optimized (see Structural Models and Potential Energy Function), heated to 150 K, and equilibrated using velocity rescaling. The simulation was then continued with a 500 ps Langevin dynamics run, which was used to derive the average coordinates of the water B oxygen atoms and the force constant k_{harm} (=0.91 kcal/mol/Å^2) according to eq 1. The location of water molecule B during the Langevin MD simulation run is indicated in Figure 1. The same protocol was used to assess the thermodynamic permissibility of a water molecule in cavity B at 300 K. A similar average location of water B was found as for 150 K, and a value of k_{harm} of 3.57 kcal/mol/Å^2.

QM/MM MD Simulations. To assess the location and the dynamics of water molecule B at 300 K in a QM/MM description, we performed an MD simulation at 300 K. As starting coordinates, we used the conformer labeled here as React-watB, pre-equilibrated at 150 K. React-watB was prepared from the cytoplasmic-oriented conformer found to be compatible with active-proton pumping[16] by changing the configuration of the active-site water molecules to mimic that from ref 14 (i.e., water molecules w401, w406, and water B are present; see Scheme 1 and Figure 1). We slowly heated React-watB from 150 to 300 K within 150 ps, and then re-equilibrated at 300 K during ~250 ps of dynamics using velocity rescaling, and 100 ps without rescaling of velocities. We used an integration step of 1 fs.

Potential of Mean Force Calculations for Proton Transfer. The potential of mean force (PMF) for proton transfer was computed by performing umbrella sampling calculations[77] in conjunction with Grossfield's implementation[78] of the weighted histogram analysis method (WHAM).[79] In umbrella sampling calculations, molecular dynamics simulations are performed with a biasing potential that confines the system in the vicinity of discrete regions of the configurational space.[80] That is, provided a reaction coordinate chosen to describe the proton-transfer event, in each consecutive simulation window one samples along a certain value of the reaction coordinate that is varied in small steps such that the system is driven from the reactant (proton on the donor group) to the product (proton on the acceptor group) states. The resulting set of data at different values of the reaction coordinate is then used in the WHAM analysis to extract the PMF.

To simplify the costly QM/MM PMF calculations, here we probed the free energy landscape for proton transfer by using the distance between the water B proton and the Asp85-$O_{\delta 1}$ atom (Scheme 1 and Figure 3B) as a reaction coordinate. To assess the convergence of the simulations, we first performed three sets of PMF computations starting from two different snapshots of simulations equilibrated at 300 K, in which water B bridges the Schiff base and Asp85. In the first two of these

TABLE 1: Free Energy for the Creation (Insertion) and Annihilation of the Cytoplasmic Water Molecule B[a]

	δt_1	δt_2	$\Delta A^{elec}_{annihil}$	$\Delta A^{vdw}_{annihil}$	$\Delta A_{annihil}$	ΔA^{elec}_{insert}	ΔA^{vdw}_{insert}	ΔA_{insert}	$\Delta\Delta A$
					150 K				
1	0.1	0.25	17.4	1.6	19.0	−11.1	−1.1	−12.2	6.8
2	1.25	0.25	15.6	1.1	16.7	−15.7	−1.3	−17.0	−0.3
3	5.0	0.25	16.3	0.3	16.6	−16.2	−0.5	−16.7	−0.1
4	10	0.25	16.7	0.8	17.5	−16.2	−0.6	−16.8	0.7
5	8	2	16.8	0.3	17.1	−16.3	−0.7	−17.0	0.1
6	20	10	16.6	1.2	17.8	−14.1	−1.4	−15.5	2.3
					300 K				
7	8	2	13.1	0.3	13.4	−11.2	−0.6	−11.8	1.6
8	20	10	13.4	0.5	13.9	−11.6	−0.4	−12.0	1.9

[a] The following notations are used: δ_1 - the equilibration time (in picoseconds) for each window (i.e., each λ value), starting from the last coordinate set of the previous window; δt_2 - the sampling time (in picoseconds) for each value of the coupling parameter λ; ΔA^{elec} - the electrostatic (Coulombic) component of the free energy; ΔA^{vdw} - the van der Waals component of the free energy; $\Delta\Delta A$ was calculated as $\Delta\Delta A = \Delta A_{annihil} - |\Delta A_{insert}|$. The subscripts *annihil* and *insert* denote the free energy for annihilating and respectively for inserting the water molecule. All free energy values are given in kcal/mol. Each free energy calculation 1−8 consisted of four simulation runs, and in each individual run, there were 10 intermediate trajectories (see Methods).

tests, we varied the origin of the harmonic potential from 1.72 to 1.0 Å as follows: (a) in 13 simulations, 40 ps each, with force constants between 100 and 600 kcal/mol·Å^2; (b) in 12 simulations, 100 ps each, with force constants between 100 and 950 kcal/mol·Å^2. The PMF barrier and reaction energy were 7.4 kcal/mol and respectively 1.3 kcal/mol in test a and 7.1 and 0.5 kcal/mol in test b. The third PMF computation (c) started from the conformer depicted in Figure 3B and consisted of 17 simulations, 50 ps each, in which the origin of the harmonic potential was varied from 1.96 to 1.0 Å with force constants between 100 and 950 kcal/mol·Å^2. Coordinates were saved at each simulation step, resulting in a set of 850.000 data sets. The PMF barrier computed using the entire data set from simulation c is 6.8 kcal/mol, and the reaction energy is −2.6 kcal/mol. When only the last 25 ps of each of the 17 windows were considered (42.500 data sets), the PMF barrier was 6.9 kcal/mol, and the reaction energy −3.1 kcal/mol. The discussion above indicates a reasonable convergence of the PMF computation. The range of force constants used in the PMF calculations here is similar to that used in other investigations of proton transfer in enzymes (e.g., 50−1000 kcal/mol·Å^2 in ref 65 and 100−500 kcal/mol·Å^2 in ref 66). In the WHAM analysis, we used a convergence criterion of 10^{-3} kcal, and estimated the statistical uncertainties of the PMF by a Monte Carlo bootstrap analysis.[78]

Results and Discussion

Free Energy for the Insertion of a Cytoplasmic Water Molecule. In the bR resting state at room temperature, the Schiff base proton and water molecule(s) at the retinal binding site exchange with the bulk,[81,82] and at least seven buried water molecules exchange with the bulk within 0.1−10 μs at 4 °C in dark-adapted bacteriorhodopsin.[41] Because in the bR resting and dark-adapted states water molecules are in thermodynamic equilibrium with the bulk, the probability of occupancy of a water molecule in any given protein site is determined by the free energy difference between the state with the hydrated site and that with the water molecule in the bulk.[23,74] However, it is not clear whether, on the microsecond time scale of the K and L intermediates, the active-site water molecules reach equilibrium with the bulk water following the structural perturbation induced by retinal photoisomerization. The probability of occupation and residence times of the active-site water molecules will depend on the free energy difference between the site with the water present and those other hydration sites in the protein that are kinetically accessible within the lifetime of the K or L states. That is, the presence and residence time of water molecule B in the L state depends on its free energy at locations in K, L, and M but also on the activation energy associated with movement of the water molecule to/from location B. In the discussion of the thermodynamic stability of hydration site B, we consider several possible alternative locations from which water molecule B might originate.

The convergence of the free energy values is indicated by the difference between the free energy for the insertion and the free energy for the annihilation of the water molecule being very small. Simulations in which the Langevin dynamics for equilibration and production for each value of the coupling parameter λ (see Methods) were performed for various lengths of time (Table 1) indicate that with too short simulation times (simulation 1 in Table 1) there is poor convergence of the electrostatic component of the free energy, leading to a significant difference (~7 kcal/mol) between the free energy of insertion and that for annihilation of the water molecule. The converged free energy value for inserting water molecule B is approximately −17 kcal/mol at 150 K and originates mainly from the electrostatic contribution (Table 1). This observation is consistent with previous calculations in which the electrostatic component was found to dominate the free energy for inserting a water molecule in the vicinity of the all-trans retinal Schiff base in the bR ground state.[23,74] At 300 K, the free energy of insertion of water B is approximately −12 kcal/mol (Table 1), also arising largely from electrostatic interactions.

The large negative free energy for inserting water molecule B indicates that the pocket on the cytoplasmic side of the retinal Schiff base provides an energetically favorable environment for stabilizing a water molecule. However, the inherent nonequilibrium nature of the pump renders the occupancy of location B dependent not only on the free energy of insertion of the water molecule but also on the thermodynamic stability of the same water molecule in its original location before it moves to the cytoplasmic location B, and on the rate-limiting barrier associated with water relocation.

A priori, at least three pathways exist leading to the occupation of location B by a water molecule. First, water molecule B may come from the cytoplasmic bulk. This possibility is supported by the observations that (i) hydration of the cytoplasmic channel in the bR state is allowed based on thermodynamic grounds;[23,74] (ii) in MD simulations, bulk water molecules visit transiently internal locations of bacteriorhodop-

sin, such that the number of internal water molecules is significantly larger than indicated by crystal structures.[42] Assuming that the energetic cost for moving a water molecule from the bulk to location B can be overcome on the ~1 μs time scale for the rise of L, then the probability of occupancy of water B calculated from eq 2 is 1 at both the 150 and 300 K temperatures.

A second putative pathway leading to the occupancy of cavity B involves relocation of a water molecule from the cytoplasmic channel of the protein. Weakly bound water molecules on the cytoplasmic side of the retinal Schiff base appear to relocate in L,[83] raising the possibility that the cytoplasmic site B might be occupied by a water molecule coming from another cytoplasmic site of bacteriorhodopsin.

The third path, and perhaps the most intriguing one, is from the extracellular side of the retinal Schiff base, with an extracellular water molecule (e.g., w402) relocating to cavity B prior to retinal deprotonation.[14] Free energy computations indicated a high probability of occupancy for w402 in the bR resting state,[23,74] and w402 is present in the high-resolution crystal structures of this intermediate state.[11,12] W402 is present in the L-state structural models from refs 13 and 28 close to its location in the bR state, but is absent in those of refs 14, 35, and 36. Molecular dynamics simulations on the nanosecond time scale suggested that the reorientation of the Schiff base toward the cytoplasmic side could be accompanied by the displacement of w402 toward a more extracellular location, i.e., further away from the retinal Schiff base.[37]

Whether or not w402 could relocate to B prior to retinal deprotonation will be determined by the free energy difference between the two end states (w402 between Asp85 and Asp212, and w402 in location B), and by the interconversion rate. Considering only two-state comparisons, the probability of occupancy of water molecule B at 150 K (the temperature at which the structure was solved) is small (17%) when computed taking a value of −16.8 kcal/mol as the free energy of insertion at its original location, as computed for the free energy of insertion of water w402 in the bR resting state;[74] at 300 K, the probability is zero (see eq 3). Molecular dynamics simulations on the bR and M intermediate states at 300 K also do not support the translocation of water w402, as no passage of water molecules from the extracellular to the cytoplasmic side past the retinal Schiff base region was observed on the nanosecond timescale.[42]

Influence of a Water Molecule Hydrogen Bonding to the Retinal Schiff Base on the Proton-Transfer Energetics. In the crystal structure of ref 14, the N−C_α−C_β−$C_{\gamma 2}$ χ1 dihedral angle of Thr89 is *trans* at −169.4° (Figure 1). In contrast, other crystal structures of bR[11,12]- and L-state structures[28,35,36] indicate the Thr89 N−C_α−C_β−$C_{\gamma 2}$ dihedral angle is *gauche* with values between −57 and −68°. The g*auche* geometry of Thr89 is consistent with an analysis of crystal structures of globular proteins, indicating the *gauche* geometry of the χ1 angle of threonine groups being strongly preferred relative to *trans* (depending on the local environment, conformations of amino acid side chains deviating from the statistically preferred rotameric state may nevertheless occur[84]).

The rotameric state of Thr89 in ref 14 allows a hydrogen bond between Thr89 and Asp85, as indicated by low-temperature FTIR spectroscopy[85] (Figure 1). However, due to the presence of the bulky methyl group of Thr89 in the vicinity of the Schiff base segment, the interaction between the Schiff base, Thr89, and water B is not optimal; it is hence unclear whether the formation of the strong Schiff base:counterion interaction indicated by NMR[15] is possible.

We tested the preferred geometry of the Thr89 side chain in the bR protein environment by performing a QM/MM CPR path calculation for the rotation of the N−C_α−C_β−$C_{\gamma 2}$ dihedral angle from *trans* to *gauche* starting from a QM/MM-optimized conformer prepared using the structure from ref 14. The computation indicated that the *gauche* geometry is strongly preferred relative to *trans*, by 12 kcal/mol, and the rate-limiting energy barrier is <2 kcal/mol. The favorable energy of the *gauche* geometry of Thr89 is explained by the more optimal hydrogen bonds of the Schiff base, water B, Thr89, and Asp85, which can hydrogen bond in the *gauche*-Thr89 geometry (see inset at $L = 0$ in Figure 2A). The result of the QM/MM calculation is consistent with the *gauche* geometry of the Thr89 N−C_α−C_β−$C_{\gamma 2}$ dihedral angle indicated in other crystal structures of bR and L states.[11,12,28,35,36] A test MM MD simulation at 300 K (heating, equilibration with velocity rescaling, and 500 ps Langevin run) indicated that the *gauche* geometry of Thr89 is stable in the structure of ref 14. The average Schiff base:water B distance in the *gauche*-Thr89 simulation is very similar to that for the *trans*-Thr89 conformer (the average water B:Schiff base nitrogen distance computed from 500 ps of Langevin run is 3.1 ± 0.3 Å in the *trans*-Thr89 simulation (Figure 1), 3.2 ± 0.3 Å for *gauche*-Thr89, and 3.3 Å in the crystal structure of ref 14). Nevertheless, consistent with the QM/MM reaction-path calculation discussed above, the Schiff base:Thr89 interaction is more favorable in the *gauche*-Thr89 than in the *trans*-Thr89 simulation: In the MM Langevin run, the average distance between the Schiff base nitrogen and the Thr89 hydroxyl oxygen is 3.4 ± 0.3 Å for the *gauche*-Thr89 geometry, as compared to 5.2 ± 0.3 Å for *trans*-Thr89.

The retinal geometry indicated by the L-state model of ref 14 is similar to the cytoplasmic-oriented conformer derived previously from reaction-path calculations.[16] We demonstrated that the cytoplasmic-oriented conformer derived from reaction-path calculations[16] is compatible with a productive proton-pumping cycle, and with site-directed mutagenesis results.[16,31] Hence, here, we investigated the influence of water molecule B on the proton-transfer energetics by using React-watB, a conformer prepared from the cytoplasmic-oriented conformer from ref 16 by considering the active-site water configuration from ref 14, and reoptimizing the geometry as detailed in Methods. In React-watB, the Thr89 N−C_α−C_β−$C_{\gamma 2}$ dihedral angle is *gauche*. The C_{12}−C_{13}=C_{14}−C_{15}, C_{13}=C_{14}−C_{15}=N, and C_{14}−C_{15}=N−C_ε dihedral angles in the QM/MM-optimized React-watB are 19.6, −158.0, and −166.0°, respectively. These values are close to those measured in the *gauche*-Thr89 QM/MM-optimized conformer prepared from the reaction-path calculation using the structure from ref 14 (described above) of 25.6, −166.3, −162.4°, respectively.

Because it is not clear whether water B originates from water w402 or from another (cytoplasmic) location, the computations in the presence of water B were performed both in the presence and in the absence of w402 (Table 2). The conformer that contains both water molecules B and w402 is denoted as React-watB-w402.

The QM/MM-optimized React-watB contains a hydrogen-bonded network (donor−acceptor distances of 2.7−2.8 Å) that connects the protonated Schiff base to the negatively charged Asp85 via water B and Thr89 (inset at $L = 0$ in Figure 2A). Relocation of water molecule B and twisting of the retinal Schiff base segment by crossing over two transition states with local

TABLE 2: Rate-Limiting Energy Barriers for Retinal Deprotonation in the Presence of a Cytoplasmic Water Molecule[a]

pathway	intermediate proton carrier	energy barrier (kcal/mol)
1a	water molecule B	10.0
1b	Thr89	21.5
1b′	Thr89	8.0
1c		18.0
1c′		15.3
2a	water molecule B and Thr89	14.1
2b	Thr89	18.3
2c		19.5

[a] Pathways **1a**, **1b**, **1b′**, **1c**, and **1c′** were computed in the presence of water molecule B and in the absence of w402. Pathways **2a**, **2b**, and **2c** were computed in the presence of both water molecules B and w402.

energy barriers of 2.4 kcal/mol ($L = 0.07$ in Figure 2A, green curve) and 4.7 kcal/mol ($L = 0.32$ in Figure 2A, green curve) lead to a low-energy conformer (denoted here as React-watB^{inter}) in which water B bridges the Schiff base and Asp85 via hydrogen-bonding interactions (inset at $L = 0.46$ in Figure 2A, green curve). React-watB^{inter} is 5.5 kcal/mol lower in energy than React-watB. From React-watB^{inter}, the transfer of the retinal Schiff base proton to Asp85 *via* water B (path **1a**) requires a rate-limiting energy barrier of 10.0 kcal/mol ($L = 0.57$ in Figure 2A, green curve). Following proton transfer, water molecule B moves by crossing over a local energy barrier of 7.2 kcal/mol ($L = 0.82$ in Figure 2A, green curve), leading to the product state in which water B hydrogen bonds to Thr89 and the deprotonated Schiff base (inset at $L = 1.0$ in Figure 2A).

Starting from React-watB^{inter} proton transfer via Thr89 (path **1b**) or via a direct jump to Asp85 (path **1c**) is unlikely given the significant rate-limiting energy barriers of 21.5 kcal/mol ($L = 0.46$ in Figure 2A, red curve) and 18.5 kcal/mol ($L = 0.5$ in Figure 2A, black curve), respectively.

We have further explored the paths for retinal deprotonation from React-watB by computing pathways for proton transfer via Thr89 or direct to Asp85 in which the low-energy conformer at $L = 0.46$ in Figure 2A is not an intermediate state (Figure 2B). We label these two additional paths **1b′** (via Thr89) and **1c′** (direct to Asp85). Path **1b′** starts with a sequence of rearrangements of water B with energy barriers of <3 kcal/mol leading to a local minimum ($0 < L < 0.35$ in Figure 2B) that has the same energy as React-watB. Proton transfer via Thr89 then occurs then by crossing over a relatively small energy barrier of 8.0 kcal/mol ($L = 0.45$ in Figure 2B. red curve). In Path **1c′** (direct proton transfer), the rate-limiting barrier is 15.3 kcal/mol ($L = 0.27$ in Figure 2B, black curve).

The smaller energy barriers for proton transfer of paths **1b′** and **1c′** relative to paths **1b** and respectively **1c** are due to the different location of water B at the transition state. In paths **1b** and **1c**, proton transfer starts from a low-energy conformer in which water B bridges the Schiff base and Asp85, hence strongly favoring path **1a** via water B (Figure 3A); proceeding with a proton transfer other than via water B requires moving water B away from its favorable location. For example, in path **1b**, at $L = 0.4$, water B hydrogen bonds to Asp85 (the distance is 2.7 Å), but the Schiff base:water B hydrogen bond has broken (3.8 Å) and the Schiff base interacts stronger with Thr89 (3.1 Å) (see also insets at $L = 0.46$ and $L = 0.5$ in Figure 2A). In paths **1b′** and **1c′**, water B remains hydrogen bonded to Thr89 (see insets in Figure 2B).

The computations discussed above indicate that, in the presence of water B and absence of a water molecule bridging Asp85 and Asp212, there exist several local minima distinguished by the retinal twist and by the Schiff base:water interactions ($0 < L < 0.46$ in Figure 2A green curve; $0 < L < 0.35$ in Figure 2B red curve); the energy barriers between these local minima range between 2.2 and 4.7 kcal/mol. The lowest-energy preproton-transfer state conformer indicated by the reaction-path calculations is React-watB^{inter} ($L = 0.46$ in Figure 2A, green curve, and Figure 3A). This conformer can be reached from React-watB by crossing over energy barriers of less than 5 kcal/mol. Starting from React-watB^{inter}, a concerted proton transfer can occur in which the water molecule receives the Schiff base proton, and gives a proton to a negatively charged Asp85 (green curve in Figure 2A).

In React-watB-w402, in which both water B and w402 are present (see inset at $L = 0$ in Figure 2C), the motions of both the retinal Schiff base and Asp85 are significantly restricted by hydrogen bonding to water. As a consequence, the direct (path **2c**) and the Thr89 (path **2b**) proton-transfer paths become unlikely, with rate-limiting barriers of 19.5 kcal/mol ($L = 0.5$ in Figure 2C, black curve) and 18.3 kcal/mol ($L = 0.39$ in Figure 2C, red curve), respectively. Instead, proton transfer occurs via a concerted mechanism involving water B and Thr89 (path **2a**), with a rate-limiting barrier of 14.1 kcal/mol ($L = 0.44$ in Figure 2C, green curve). In the deprotonated retinal Schiff base/protonated Asp85 state, the Schiff base remains hydrogen bonded to the cytoplasmic water molecule (inset at $L = 1$ in Figure 2C).

Previous calculations performed in the presence of water w402 and in the absence of water B indicated that proton transfer may occur not only on the Thr89 side of the retinal but also on the Asp212 side.[16] The calculated rate-limiting barrier for proton transfer on the Asp212 side of the retinal is 11.5 kcal/mol,[16] close to the experimental enthalpy of activation of ~13 kcal/mol.[68] In the presence of water B hydrogen bonding to the Schiff base, the twisting of the retinal Schiff base (with w402 present) toward Asp212, as required for proton transfer on that side of the retinal,[16] is hindered due to the cytoplasmic orientation of the retinal Schiff base being largely favored (by ~16 kcal/mol). As a consequence, the Asp212 path is no longer followed.

The reaction-path calculations discussed above indicate that the presence of a water molecule within hydrogen-bonding distance of the retinal Schiff base has the potential to direct the proton-transfer path along the Thr89 side of the retinal. In the presence of water B, proton transfer occurs via water B and Thr89, when w402 is present (path **2a**), or via the bridging water molecule B, when 402 is absent from its location between Asp85 and Asp212 (path **1a**).

Hydrogen Bonding to Water Affects Retinal Geometry and Dynamics. The presence of hydrogen bonds connecting the protonated retinal Schiff base to the negatively charged Asp85 via water molecule B in the low-energy intermediate state React-watB^{inter} (Figure 3A; inset at $L = 0.46$ in Figure 2A) is consistent with suggestions from NMR spectroscopy of a strong interaction between the retinal Schiff base and its counterion.[15,27] Moreover, the observation that a water molecule remains hydrogen bonded to the deprotonated retinal Schiff base after completion of proton transfer ($L = 1$ in Figure 2A) is consistent with suggestions from NMR that in M the Schiff base is hydrogen bonded.[15,27] Water molecules can however be very dynamic, and their dynamical motions may have a significant influence on proton-transfer reactions.[64] To further investigate the effect of water molecule B on the Schiff base's dynamics and deprotonation reaction, we performed QM/MM molecular dynamics and test PMF calculations.

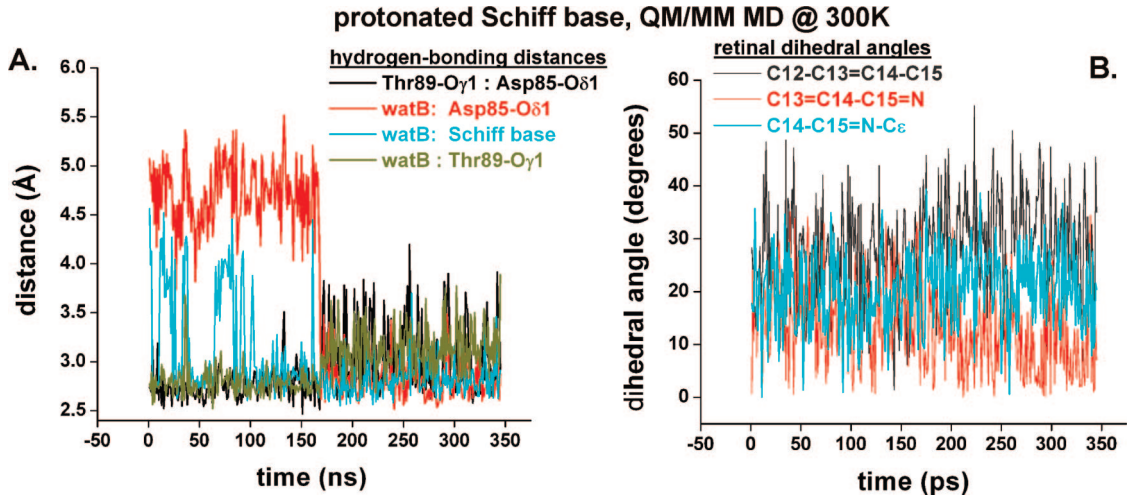

Figure 4. Dynamics of the retinal dihedral angles and active-site hydrogen bonds. (A) Time evolution of hydrogen-bonding interactions between the Schiff base and water w402 (cyan), water B and Asp85 (red), water B and Thr89 (olive), and between Asp85 and Thr89 (gray). (B) Time evolution of the dihedral angles C_{12}—C_{13}=C_{14}—C_{15}, C_{13}=C_{14}—C_{15}=N, and C_{14}—C_{15}=N—Cε depicted in gray, red, and cyan, respectively. Distances are given in angstroms, and dihedral angles in degrees.

Early during the first ~160 ps of QM/MM equilibration at 300 K, water molecule B sampled locations very similar to those at $L = 0$ in Figure 2A and B, and $L = 0.35$ in Figure 2B red curve (see insets in Figure 2A and B). This dynamics of water molecule B is illustrated in Figure 4A by the distance between the Schiff base and water B (cyan curve in Figure 4A) sampling hydrogen-bond values (geometries similar to that at $L = 0$ in Figure 2A,B), and values larger than hydrogen-bonding distances (geometries similar to that at $L = 0.35$ in Figure 2B, red curve), while water B remains hydrogen bonded to Thr89 (olive curve in Figure 4A). Water molecule B then relocated and remained stable in a bridging location between the Schiff base and Asp85 (Figure 3B; red and cyan curves in Figure 4A). The onset of hydrogen bonding between water B and Asp85 leads to weakening of the Thr89:Asp85 hydrogen bond, which is stable before relocation of water B but rapidly breaks and reforms after relocation of the water molecule (black curve in Figure 4A). The relatively large range of values sampled by the retinal dihedral angles (Figure 4B) is consistent with previous observations from MD simulations indicating significant flexibility of the retinal chain.[36,43,44,86]

The conformer at the end of the 350 ps equilibration at 300 K is denoted here as React-watB$^{300\,K}$ (Figure 3B). The geometry of water B in React-watB$^{300\,K}$ is very similar to that from the low-energy intermediate React-watB^{inter} found along the minimum-energy path (Figure 3). The good qualitative agreement between the preferred location of water B in the QM/MM reaction-path and MD simulations is encouraging for the sampling of the configurational space performed with the reaction-path computations. Importantly, the QM/MM MD simulations support the observation from reaction-path calculations that proton transfer in the presence of a cytoplasmic water molecule is likely to start from a conformer in which the water molecule bridges the twisted retinal Schiff base and the negatively charged Asp85.

The roughness of the minimum-energy potential surface indicated by the presence of energy minima (distinguished by the Schiff base/water B/Asp85 interactions) on the preproton-transfer state segment of the path ($0 < L < 0.46$ in Figure 2A; $0 < L < 0.35$ in Figure 2B, red curve) is consistent with observations from NMR that, at cryogenic temperatures, the energy landscape of the L state is rugged.[15] In a test ~550 ps QM/MM MD simulation at 210 K, the temperature used to trap an early-M state,[87] we observed sampling of conformers similar to those at $L = 0$ in Figure 2A,B, and at $L = 0.35$ in Figure 2B. The QM/MM MD simulations at 300 K (Figure 4) indicate that, unlike at low temperatures, at room temperature, the formation of a stable structure in which the Schiff base and water B are bridged by a water molecule (Figure 3B) is barrierless at this temperature.

The hydrogen bonding between the twisted Schiff base, w402, and the negatively charged Asp85, may be even stronger than in conformers React-watB^{inter} and React-watB$^{300\,K}$, because SCC-DFTB overestimates the hydrogen-bonding distance of the retinal Schiff base (i.e., it underestimates the hydrogen-bonding strength). In fully optimized SCC-DFTB/MM and B3LYP 6-31G**/MM geometries, the hydrogen-bonding distance between the protonated Schiff base and the Thr89 hydroxyl group was ~0.11 Å longer with SCC-DFTB than with B3LYP/6-31G**.[20] Finally, we note the limitation of the classical force field in describing the Schiff base:water interactions. With MM, the water molecule remained hydrogen bonded to the retinal Schiff base in the cytoplasmic location (Figure 1); the QM/MM computations indicate that the geometry in which the water bridges the Schiff base and Asp85 is energetically favored. The difference between the MM and QM/MM descriptions is likely to arise from the limitations of the classical force field in describing the retinal twist and the strong hydrogen-bonding interactions in the Schiff base region. Prolonged QM/MM MD simulations may be necessary to fully explore the possible locations of water molecules in the active site, and how they interact with retinal and protein groups.

PMF of Proton Transfer from the Schiff Base to Asp85 via the Water Molecule. In previous computations, we have shown that the transfer of the proton from the retinal Schiff base can involve a complex combination of motions of the retinal, protein groups, and water molecules.[16,20] This complexity can make the choice of a proper reaction coordinate to describe the proton-transfer event very difficult.[20,72] The geometry of the retinal Schiff base, Asp85, and the intervening water molecule B in the QM/MM simulation at 300 K (Figures 3B and 4) is consistent with a concerted proton-transfer path via water B, as indicated by the reaction-path calculations in which no *a priori* definition of the reaction coordinate was used (Figure 2A).

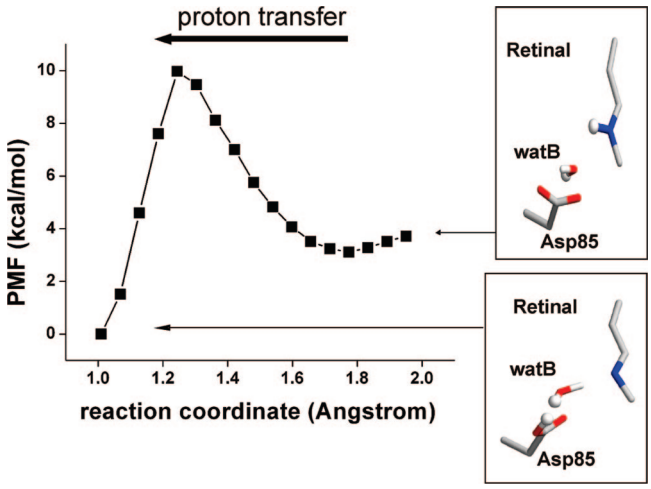

Figure 5. PMF for proton transfer from the Schiff base to Asp85. The reaction coordinate is the distance between the water proton and the Asp85-$O_{\delta 1}$ atom. Seventeen simulations were performed, in which the origin of the harmonic potential was varied from 1.96 to 1.0 Å, for a total of 850 ps. For each window, the first 25 ps were considered equilibration and the remaining 25 ps were used to compute the PMF (425.000 data sets). Insets show schematic representations of the retinal Schiff base, Asp85, and the bridging water molecule B at the beginning (protonated Schiff base, negatively charged Asp85) and at the end (neutral Schiff base/Asp85) of the PMF computation.

The test PMF computations indicate that proton transfer from water B to Asp85 is accompanied by the transfer of a proton from the Schiff base to water B (Figure 5). The PMF computed by using as starting coordinates the conformer at the end of the simulation equilibrated at 300 K (Figure 3B) has an associated free energy barrier of ~7 kcal/mol, and a reaction free energy of −3.1 kcal/mol (Figure 5). That is, both the PMF (Figure 5) and the reaction-path computations (green curve in Figure 2A) indicate that proton transfer from the Schiff base to Asp85 via the bridging water molecule is compatible with the ~10 μs time scale of the L-to-M transition. Following proton transfer, water molecule B remains hydrogen bonded to the retinal Schiff base (see insets in Figure 5). The presence of a hydrogen bond between the deprotonated retinal Schiff base and the water molecule in the PMF (Figure 5) and the reaction-path calculations (Figure 2) is consistent with the NMR data indicating that in M the deprotonated retinal Schiff base has a hydrogen-bonding partner.[15,27]

Influence of Active-Site Hydrogen-Bonding Interactions on Bacteriorhodopsin Proton-Transfer Energetics. The significant influence of water molecules on the proton-transfer energetics discussed here and elsewhere[16,18−20,30] suggests that the dynamics of the water molecules and retinal leading to fluctuations in the pattern and strength of the active-site hydrogen bonds could determine the pathway followed during the first proton-transfer step. The critical role of the active-site water molecules in proton-transfer energetics adds to the complexity of the reaction paths in enzymes with many degrees of freedom, in which more than a single path may be available for the reaction.[16]

To illustrate how water molecules hydrogen bonding to the proton donor and acceptor groups can influence the proton-transfer energetics, we constructed a diagram (Figure 6) that is based on pathways discussed here and in our previous work.[16,30,31,88] Due to the prohibitive computational costs, we cannot perform QM/MM MD and PMF calculations for all possible pathways of the various active-site configurations. The diagram illustrates the effect of water molecules on the energetics of proton transfer and retinal configurational changes, as indicated by the reaction-path calculations. The comparison of the reaction-path and MD simulations presented here indicates that the minimum-energy reaction-path computations give a good representation of the possible geometries of the active site. The presence, in some of the reaction paths, of several local minima distinguished by the Schiff base:water interactions (Figure 2A,B) suggests that the preferred geometry may also depend on the temperature.

For completeness, the diagram of the reaction paths (Figure 6) includes a test calculation from K[48,88] to the cytoplasmic-oriented preproton-transfer state conformer in the absence of water molecule w402. We also attempted to perform proton-transfer calculations using the highly twisted extracellular-oriented putative L-state model of ref 13. However, although a very careful QM/MM energy optimization protocol was used (see Methods), the retinal appeared to prefer a bR-like all-trans geometry. This could be explained by the C_{12}−C_{13}=C_{14}−C_{15} dihedral angle in the crystal structure of ref 13 being −107.9°, i.e., already past the 90°-twisted geometry of the transition to all-trans.

Water molecules can enable bridged donor−acceptor structures from which proton transfer can occur at a low energetic cost (green curve in Figure 2A; Figure 3), but they can also increase the proton-transfer barrier by restricting the motions of the proton donor and acceptor groups to which they hydrogen bond. For example, the rate-limiting barrier for the direct proton-transfer pathway from the 13-cis, 14-trans, 15-anti, cytoplasmic-oriented conformer is ~6 kcal/mol in the absence of water w402 and water B.[16] When w402 hydrogen bonds to Asp85 and restricts the motion of the Asp85 side chain, the proton-transfer barrier increases to ~12 kcal/mol.[16] The energy barrier increases further to ~20 kcal/mol when both the proton donor and acceptor groups hydrogen bond to water molecules.

Water molecules hydrogen bonding to the reacting groups can change the preferred reaction pathway. Whereas in the absence of water molecule B proton transfer can occur on either the Thr89 or the Asp212 side of the retinal,[16] in the presence of water B, proton transfer occurs only on the Asp212 side.

The role of local flexibility underlined by the computations with different active-site water molecules is also illustrated by work on the Thr89Val[16] and Asp85Glu[31] mutants. It has been shown that in the Thr89Val mutant flexibility of the proton donor and acceptor groups enables direct proton transfer with a rate-limiting barrier of 12.3 kcal/mol (i.e., close to the value in the wild type).[16] Due to the enhanced flexibility of the glutamate side chain, in the Asp85Glu mutant, the direct proton-transfer path is associated with a rate-limiting barrier of 7.6 kcal/mol, which is ~5 kcal/mol less than in wild-type bacteriorhodopsin.[31] These results are consistent with the experimental observations that the Thr89Val mutant has wild-type levels of retinal deprotonation,[89] and deprotonation occurs much faster in the Glu85 mutant than in the wild type.[90]

Following retinal deprotonation, relocation of water molecules on the extracellular side of the retinal Schiff base can contribute to the directionality of the proton-pumping cycle by hindering a back proton transfer from Asp85 to the retinal Schiff base.[20] Some of the crystal structures of M[22,91,92] do not indicate coordinates for w402, or w406/w402. Relative to the case where w401/w402/w406 are present in the active site, in the absence of w402 or w401/w402, the reaction energy for the back proton transfer from Asp85 to the retinal Schiff base increases by 2 and 4 kcal/mol, respectively.[20]

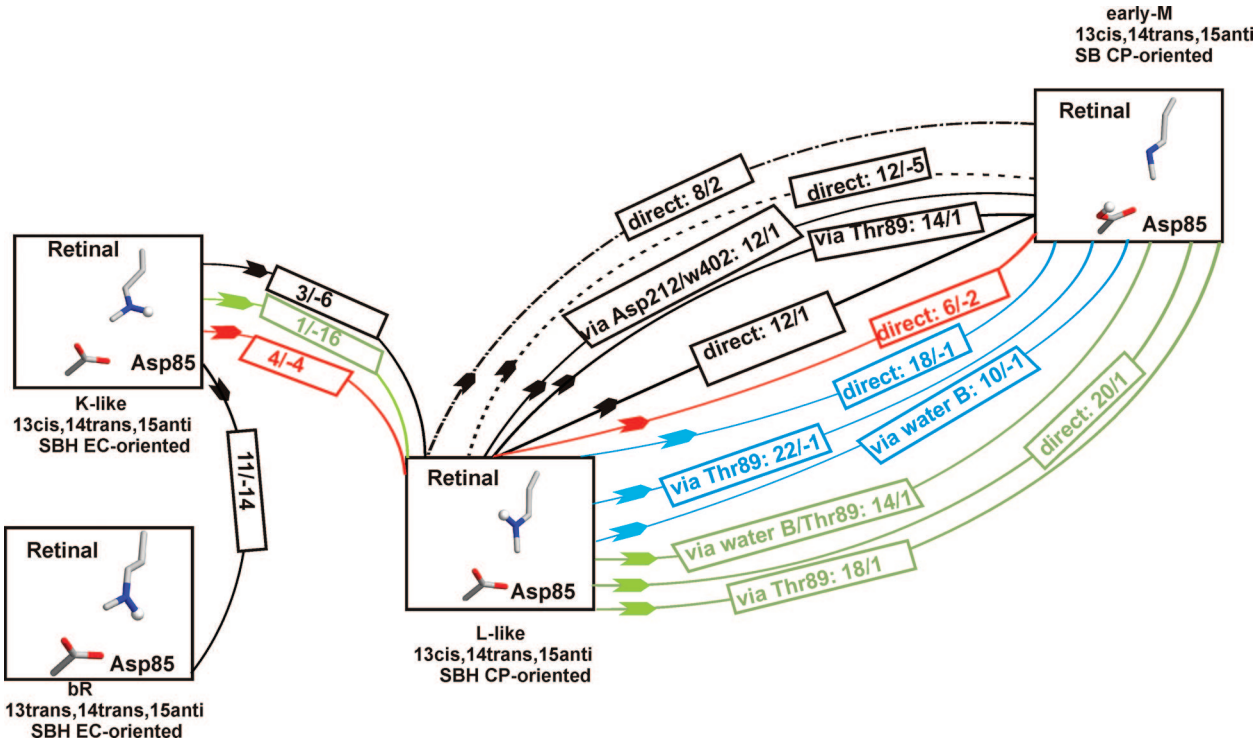

Figure 6. Effect of water molecule location on the energetics of retinal deprotonation. Each line indicates a reaction pathway. Black - paths computed in the presence of w402 for the wild type (continuous lines), Thr89Val (broken line), and Asp85Glu (dot-broken lines) mutants; red - pathways computed in the absence of w402; blue - pathways computed in the absence of w402 and in the presence of water B (with React-watB^{inter} (Figure 3A) as an intermediate conformer); green - pathways computed in the presence of w402 and water B. The arrows point to the product states. The boxes along each line give the intermediate proton carrier, and the rate-limiting barrier/the reaction energy associated with that path (SCC-DFTB/MM-optimized values, in kcal/mol). The end states are indicated schematically by the retinal/Asp85 relative orientation. The energy profiles are discussed here and in refs 16, 30, 31, and 88. Molecular movies of some of the paths included in the diagram are available at http://www.iwr.uni-heidelberg.de/groups/biocomp/fischer.

Conclusions

Water molecules hydrogen bonding to proton donor and acceptor groups affect significantly the proton-transfer energetics, and can determine which of the (multiple) reaction pathways available in the complex environment of an enzyme will be followed. When studying reaction mechanisms, it is essential to know the location of internal water molecules, and to dissect their role in the reaction energetics.

Computer simulations have indicated that small perturbations are sufficient to induce penetration of water and filling of a nanopore.[93] In the case of bacteriorhodopsin, reorientation of the retinal Schiff base from the extracellular side in bR toward the cytoplasmic side in L[14,16,36] can provide the polar interaction (the protonated retinal Schiff base) necessary to stabilize one or more water molecules in the cytoplasmic proton channel. The computations presented here indicate that the presence of water molecule B on the cytoplasmic side of the retinal Schiff base is energetically feasible. The electrostatic contribution to the stabilization of a water molecule in cavity B with the Schiff base oriented toward the cytoplasmic side is 3−7 kcal/mol larger than the value computed for a water molecule confined to location B in the bR resting state, i.e., in the absence of the stabilizing interaction with the protonated Schiff base.[74] The proposal that the interaction with the retinal Schiff base can stabilize a cytoplasmic water molecule is also supported by the coupling between water location and retinal geometry.[94]

Whether or not water molecule B is present depends on the free energy of insertion in its locations in the previous steps of the reaction cycle, and on whether the rate-limiting barrier for the relocation of the water to location B can be overcome on the time scale of the K-to-L transition. The presence of water B enables the formation of strong Schiff base:counterion interactions, hinders proton transfer on the Asp212 side of the retinal, and directs the transfer on the Thr89 side of the retinal. The dramatic effect of a single water molecule on the mechanism of proton transfer in bacteriorhodopsin highlights the crucial importance of accurate information on the location and residence times of internal water molecules for understanding proton pumps.

Acknowledgment. This work has been supported in part by the Deutsches Krebsforschungszentrum and by the Deutsches Forschungsgemeinshaft (SM 63/7). J.C.S. was supported by a United States Department of Energy Laboratory-Directed Research and Development grant. A.-N.B. is supported by grant GM74637 from the National Institutes of General Medical Sciences. A.-N.B. thanks Profs. Judith Herzfeld, Tsutomu Kouyama, and Akio Maeda for valuable discussions on the role of water molecules in bacteriorhodopsin function, and Dr. Haobo Guo for valuable advice on the PMF calculations.

References and Notes

(1) Swanson, J. M. J.; Maupin, C. M.; Chen, H.; Petersen, M. K.; Xu, J.; Wu, Y.; Voth, G. A. *J. Phys. Chem. B* **2007**, *111*, 4300–4314.

(2) Gennis, R. B. *Proc. Natl. Acad. Sci. U.S.A.* **1998**, *95*, 12747–12749.

(3) Seibold, S. A.; Mills, D. A.; Ferguson-Miller, S.; Cukier, R. I. *Biochemistry* **2005**, *44*, 10475–10485.

(4) Dencher, N. A.; Sass, H. J.; Büldt, G. *Biochim. Biophys. Acta* **2000**, *1460*, 192–203.

(5) Wikström, M.; Verkhovsky, M. I.; Hummer, G. *Biochim. Biophys. Acta* **2003**, *1604*, 61–65.

(6) Mulkidjanian, A. Y.; Heberle, J.; Cherepanov, D. A. *Biochim. Biophys. Acta* **2006**, *1757*, 913–930.
(7) Namslauer, A.; Lepp, H.; Brändén, M.; Jasaitis, A.; Verkhovsky, M. I.; Brzezinski, P. *J. Biol. Chem.* **2007**, *282*, 15148–15158.
(8) Garczarek, F., K; Gerwert, K. *Nature* **2006**, *439*, 109–112.
(9) Kandori, H. *Biochim. Biophys. Acta* **2004**, *1658*, 72–79.
(10) Oesterhelt, D.; Stoeckenius, W. *Proc. Natl. Acad. Sci. U.S.A.* **1973**, *70*, 2853–2857.
(11) Luecke, H.; Schobert, B.; Richter, H.-T.; Cartailler, J.-P.; Lanyi, J. K *J. Mol. Biol.* **1999**, *291*, 899–911.
(12) Belrhali, H.; Nollert, P.; Royant, A.; Menzel, C.; Rosenbuch, J. P.; Landau, E. M.; Pebay-Peyroula, E. *Structure* **1999**, *7*, 909–917.
(13) Lanyi, J. K.; Schobert, B. *J. Mol. Biol.* **2007**, *365*, 1379–1392.
(14) Kouyama, T.; Nishikawa, T.; Tokuhisa, T.; Okumura, H. *J. Mol. Biol.* **2004**, *335*, 531–546.
(15) Mak-Jurkauskas, M. L.; Bajaj, V. S.; Hornstein, M. K.; Belenky, M.; Griffin, R. G.; Herzfeld, J. *Proc. Natl. Acad. Sci. U.S.A.* **2008**, *105*, 883–888.
(16) Bondar, A.-N.; Elstner, M.; Suhai, S.; Smith, J. C.; Fischer, S. *Structure* **2004**, *12*, 1281–1288.
(17) Morgan, J. E.; Gennis, R. B.; Maeda, A. *Photochem. Photobiol.*, in press.
(18) Murata, K.; Fujii, Y.; Enomoto, N.; Hata, M.; Hoshino, T.; Tsuda, M. *Biophys. J.* **2000**, *79*, 982–991.
(19) Hayashi, S.; Ohmine, I. *J. Phys. Chem. B* **2000**, *104*, 10678–10691.
(20) Bondar, A.-N.; Suhai, S.; Fischer, S.; Smith, J. C.; Elstner, M. *J. Struct. Biol.* **2007**, *157*, 454–469.
(21) Schobert, B.; Brown, L. S.; Lanyi, J. K. *J. Mol. Biol.* **2003**, *330*, 553–570.
(22) Sass, H. J.; Büldt, G.; Gessenich, R.; Hehn, D.; Neff, D.; Schlesinger, R.; Berendzen, J.; Ormos, P. *Nature* **2000**, *406*, 649–653.
(23) Roux, B.; Nina, M.; Pòmes, R.; Smith, J. C. *Biophys. J.* **1996**, *71*, 670–681.
(24) Mathias, G.; Marx, D. *Proc. Natl. Acad. Sci. U.S.A.* **2007**, *104*, 6980–6985.
(25) Braun-Sand, S.; Sharma, P. K.; Chu, Z. T.; Pisklіakov, A. V.; Warshel, A. *Biochem. Biophys. Acta* **2008**, *1777*, 441–452.
(26) Lórenz-Fonfria, V. A.; Furutani, Y.; Kandori, H. *Biochemistry* **2008**, *47*, 4071–4081.
(27) Herzfeld, J.; Lansing, J. C. *Annu. Rev. Biophys. Biomol. Struct.* **2002**, *31*, 73–95.
(28) Lanyi, J. K.; Schobert, B. *J. Mol. Biol.* **2003**, *328*, 439–450.
(29) Fodor, S. P. A.; Ames, J. B.; Gebhard, R.; van der Berg, E. M. M.; Stoeckenius, W.; Lugtenburg, J.; Mathies, R. A. *Biochemistry* **1988**, *27*, 7097–7101. Ames, J. B.; Fodor, S. P. A.; Gebhard, R.; Raap, J.; van der Berg, E. M. M.; Lugtenburg, J.; Mathies, R. A. *Biochemistry* **1989**, *28*, 3681–3687.
(30) Bondar, A.-N.; Fischer, S.; Smith, J. C.; Elstner, M.; Suhai, S. *J. Am. Chem. Soc.* **2004**, *126*, 14668–14677.
(31) Bondar, A.-N.; Smith, J. C.; Fischer, S. *Photochem. Photobiol. Sci.* **2006**, *5*, 547–552.
(32) Berman, H. M.; Westbrook, J.; Feng, Z.; Gilliland, G.; Bhat, T. N.; Weissig, H.; Shinsyalov, I. N.; Bourne, P. E. *Nucleic Acid Res.* **2000**, *28*, 235–242.
(33) Morgan, J. E.; Vakkasoglu, A. S.; Gennis, R. B.; Maeda, A. *Biochemistry* **2007**, *46*, 2787–2796.
(34) Tóth-Boconádi, R.; Dér, A.; Taneva, S. G.; Keszthlyi, L. *Biophys. J.* **2006**, *90*, 2651–2655.
(35) Royant, A.; Edman, K.; Ursby, T.; Peyroula, E. P.; Landau, E. M.; Neutze, R. *Nature* **2000**, *406*, 645−648.
(36) Edman, K.; Royant, A.; Larsson, G.; Jacobson, F.; Taylor, T.; van der Spoel, D.; Landau, E. M.; Pebay-Peyroula, E.; Neutze, R. *J. Biol. Chem.* **2004**, *279*, 2147–2158.
(37) Hayashi, S.; Tajkhorshid, E.; Schulten, K. *Biophys. J.* **2002**, *83*, 1281–1297.
(38) Wood, K.; Plazanet, M.; Gabel, F.; Kessler, B.; Oesterhelt, D.; Tobias, D. J.; Zaccai, G.; Weik, M. *Proc. Natl. Acad. Sci. U.S.A.* **2008**, *104*, 18049–18054.
(39) Quillin, M. L.; Wingfield, P. T.; Matthews, B. W. *Proc. Natl. Acad. Sci. U.S.A.* **2006**, *103*, 19749–19753.
(40) Levitt, M.; Park, B. H. *Structure* **1993**, *1*, 223–226.
(41) Gottschalk, M.; Dencher, N. A.; Halle, B. *J. Mol. Biol.* **2001**, *311*, 605–621.
(42) Grudinin, S.; Büldt, G.; Gordeliy, V.; Baumgartner, A. *Biophys. J.* **2005**, *88*, 3252–3261.
(43) Lemaître, V.; Yeagle, P.; Watts, A. *Biochemistry* **2005**, *44*, 12667–12680.
(44) Tajkhorshid, E.; Baudry, J.; Schulten, K.; Suhai, S. *Biophys. J.* **2000**, *78*, 683–693.
(45) Lau, P.-W.; Grossfield, A.; Feller, S. E.; Pitman, M. C.; Brown, M. F. *J. Mol. Biol.* **2007**, *372*, 906–917.
(46) Warshel, A. *Photochem. Photobiol.* **1979**, *30*, 285–290.
(47) Edman, K.; Nollert, P.; Royant, A.; Belrhali, H.; Pebay-Peyroula, E.; Hajdu, J.; Neutze, R.; Landau, E. M. *Nature* **1999**, *401*, 822–826.
(48) Schobert, B.; Cupp-Vickery, J.; Hornak, V.; Smith, S. O.; Lanyi, J. K. *J. Mol. Biol.* **2002**, *321*, 715–726.
(49) Brooks, B. R.; Bruccoleri, R. E.; Olafson, B. D.; States, D. J.; Swaminathan, S.; Karplus, M. *J. Comput. Chem.* **1983**, *4*, 187–217.
(50) Metz, G.; Siebert, F.; Engelhard, M. *FEBS Lett.* **1992**, *303*, 237–241.
(51) Brown, L. S.; Sasaki, J.; Kandori, H.; Maeda, A.; Needleman, R.; Lanyi, J. K. *J. Biol. Chem.* **1995**, *270*, 27122–27126.
(52) MacKerell, A. D., Jr.; Bashford, D.; Bellott, R. L.; Dunbrack, R. L., Jr.; Evanseck, J. D.; Field, M. J.; Fischer, S.; Gao, J.; Guo, H.; Ha, S.; Joseph-McCarthy, D.; Kuchnir, L.; Kuczera, K.; Lau, F. T. K.; Mattos, C.; Michnick, S.; Ngo, T.; Nguyen, D. T; Prodhom, B.; Reiher, W. E., III; Roux, B.; Schlenkrich, M.; Smith, J. C.; Stote, R.; Straub, J.; Watanabe, M.; Wiorkiewicz-Kuczera, J.; Yin, D.; Karplus, M. *J. Phys. Chem. B* **1998**, *102*, 3586–3616.
(53) Jorgensen, W.; Chandrasekhar, J.; Madura, J.; Impey, R.; Klein, M. *J. Comput. Chem.* **1983**, *79*, 926–935.
(54) Gruia, A. D.; Bondar, A.-N.; Smith, J. C.; Fischer, S. *Structure* **2005**, *13*, 617–627.
(55) Nina, M.; Roux, B.; Smith, J. C. *Biophys. J.* **1995**, *68*, 25–39.
(56) Field, M. J.; Bash, P. A.; Karplus, M. *J. Comput. Chem.* **1990**, *11*, 700–733.
(57) Singh, U. C.; Kollman, P. *J. Comput. Chem.* **1986**, *7*, 718–730.
(58) Warshel, A. *Computer modeling of chemical reactions in enzymes and solutions*; John Willey & Sons: New York, 1991.
(59) Neria, E.; Fischer, S.; Karplus, M. *J. Chem. Phys.* **1996**, *105*, 1902–1921.
(60) Elstner, M.; Porezag, D.; Jungnickel, G.; Elner, J.; Haugk, M.; Frauenheim, T.; Suhai, S.; Seifert, G. *Phys. Rev. B* **1998**, *58*, 7260–7268.
(61) Cui, Q.; Elstner, M.; Kaxiras, E.; Frauenheim, T.; Karplus, M. *J. Phys. Chem. B* **2001**, *105*, 569–585.
(62) Elstner, M.; Frauenheim, T.; Kaxiras, E.; Seifert, G.; Suhai, S. *Phys. Status Solidi B* **2000**, *217*, 357–376.
(63) Zhou, H.; Tajkhosrhid, E.; Frauenheim, T.; Suhai, S.; Elstner, M. *Chem. Phys.* **2002**, *277*, 91–103.
(64) Riccardi, D.; König, P.; Guo, H.; Cui, Q. *Biochemistry* **2008**, *47*, 2369–2378.
(65) Xu, Q.; Guo, H.; Gorin, A.; Guo, H. *J. Phys. Chem. B* **2007**, *111*, 6501–6506.
(66) Guo, H.; Rao, N; Xu, N.; Guo, H. *J. Am. Chem. Soc.* **2005**, *127*, 3191–3197.
(67) Subramaniam, S.; Lindahl, M.; Bullough, P; Faruki, A. R.; Tittor, J.; Oesterhelt, D.; Brown, L.; Lanyi, J. K; Henderson, R. *J. Mol. Biol.* **1999**, *287*, 145–161.
(68) Ludman, K.; Gergely, C.; Váró, G. *Biophys. J.* **1998**, *75*, 3110–3119.
(69) Fischer, S.; Karplus, M. *Chem. Phys. Lett.* **1992**, *194*, 252–261.
(70) Fischer, S.; Windshügel, B.; Horak, D.; Holmes, K. C.; Smith, J. C. *Proc. Natl. Acad. Sci. U.S.A.* **2005**, *102*, 6873–6878.
(71) Schwarzl, S. M.; Smith, J. C.; Fischer, S. *Biochemistry* **2006**, *45*, 5830–5847.
(72) Bondar, N; Elster, M.; Fischer, S.; Smith, J. C.; Suhai, S. *Phase Transitions* **2004**, *77*, 47–52.
(73) Nina, M.; Smith, J. C.; Roux, B. *J. Mol. Struct. (Theochem)* **1993**, *286*, 231–245.
(74) Baudry, J.; Tajkhorshid, E.; Molnar, F.; Phillips, J.; Schulten, K. *J. Phys. Chem. B* **2001**, *105*, 905–918.
(75) Kirkwood, J. G. *J. Chem. Phys.* **1935**, *3*, 300–313.
(76) Kollman, P. *Chem. Rev.* **1993**, *93*, 2395–2417.
(77) Torrie, G. M.; Valleau, J. P. *Chem. Phys. Lett.* **1974**, *28*, 578–581.
(78) Grossfield, A.http://membrane.urmc.rochester.edu/Grossfield_Lab/Software.html.
(79) Kumar, S.; Rosenberg, J.; Bouzida, D.; Swendsen, R. H.; Kollman, P. A. *J. Comput. Chem.* **1995**, *16*, 1339–1350.
(80) Roux, B. *Comput. Phys. Commun.* **1995**, *91*, 275–282. Souaille, M.; Roux, B. *Comput. Phys. Commun.* **2001**, *135*, 40–57.
(81) Harbison, G. S.; Roberts, J. E.; Herzfeld, J.; Griffin, R. G. *J. Am. Chem. Soc.* **1988**, *110*, 7221–7223.
(82) Deng, H.; Huang, L.; Callender, R.; Ebrey, T. *Biophys. J.* **1994**, *66*, 1129–1136.
(83) Maeda, A.; Herzfeld, J.; Belenky, M.; Needleman, R.; Gennis, R. B.; Balashov, S. P.; Ebrey, T. G. *Biochemistry* **2003**, *42*, 14122–14129.
(84) Schrauber, H.; Eisenhaber, F.; Argos, P. *J. Mol. Biol.* **1993**, *230*, 592–612.
(85) Kandori, H.; Yamazaki, Y.; Schichida, Y.; Raap, J.; Lugtenburg, J.; Belenky, M.; Herzfeld, J. *Proc. Natl. Acad. Sci. U.S.A.* **2001**, *98*, 1571–1576.
(86) Okada, T.; Sugihara, M.; Bondar, A.-N.; Elstner, M.; Entel, P.; Buss, V. *J. Mol. Biol.* **2004**, *342*, 571–583.
(87) Lanyi, J. K.; Schobert, B. *J. Mol. Biol.* **2007**, *321*, 727–737.

(88) Bondar, A.-N.; Fischer, S.; Suhai, S.; Smith, J. C. *J. Phys. Chem. B* **2005**, *109*, 14786–14788.

(89) Marti, T.; Otto, H.; Mogi, T.; Rösselet, S. J.; Heyn, M. P.; Khorana, H. G. *J. Biol. Chem.* **1991**, *266*, 6919–6927.

(90) Heberle, J.; Oesterhelt, D.; Dencher, N. A. *EMBO J.* **1993**, *12*, 3721–3727. Butt, H. J.; Fendler, K.; Bamberg, E.; Tittor, J.; Oesterhelt, D. *EMBO J.* **1989**, *8*, 1657–1663. Otto, H.; Marti, T.; Heyn, P. *Proc. Natl. Acad. Sci. U.S.A.* **1990**, *87*, 1018–1022. Lany, J. K.; Tittor, J; Váró, G.; Kripphl, G.; Oesterhelt, D *Biochim. Biophys. Acta* **1992**, *1099*, 102–110. Greenhalgh, D. A.; Subramaniam, S.; Alexiev, U.; Otto, H.; Heyn, M. P.; Khorana, H. G. *J. Biol. Chem.* **1992**, *267*, 25734–25738.

(91) Takeda, K.; Matsui, Y.; Kamiya, N.; Adachi, S.; Okumura, H.; Kouyama, T. *J. Mol. Biol.* **2004**, *341*, 1023–1037.

(92) Luecke, H. *Biochim. Biophys. Acta* **2000**, *1460*, 133–156.

(93) Hummer, G. *Mol. Phys.* **2007**, *105*, 201–207.

(94) Maeda, A.; Tomson, F. L.; Gennis, R. B.; Ebrey, T. G.; Balashov, S. P. *Biochemistry* **1999**, *38*, 8800–8807.

(95) Humphrey, W.; Dalke, A., K; Schulten, K. *J. Mol. Graphics* **1996**, *14.1*, 33–38.

JP801916F